Performance of CdS/CdSe/ZnS quantum dot-sensitized TiO_2 mesopores for solar cells

Tung Ha Thanh[1*], Quang Vinh Lam[2], Thai Hoang Nguyen[2], and Thanh Dat Huynh[3]

[1]*Faculty of Physics, Dong Thap University, Dong Thap Province, Vietnam*

[2]*University of Science, Viet Nam National University, Ho Chi Minh City, Vietnam*

[3]*Viet Nam National University, Ho Chi Minh City, Vietnam*

[*]*Corresponding author: tunghtvlcrdt@gmail.com*

Received February 19, 2013; accepted April 3, 2013; posted online July 3, 2013

We prepare CdS/CdSe/ZnS thin films by successive ionic layer adsorption and reaction method. Results show a wider photoresponse range of TiO_2 mesopores from the ultraviolet region to the visible light region. Sequentially assembled CdS/CdSe/ZnS quantum dots exhibit significantly improved light-harvesting ability and photocurrent efficiency. A high efficiency of 1.059354% is obtained.

OCIS codes: 250.0250, 260.0260.

doi: 10.3788/COL201311.072501.

Numerous techniques can be used to synthesize semiconductor quantum dots (QDs), such as reverse micelle[1], epitaxial, colloidal, and hydrothermal methods[2,3], depending on the application. QDs have potential applications in thin film light-emitting devices, nonlinear optical devices, fluorescent labels for biological applications[4,5], solar cells, displays, sensors or biosensors, and lasers. Numerous high-quality QDs, such as CdS[6,7], CdSe[8,9], and CdTe, have been successfully synthesized.

In this letter, CdSe QDs and TiO_2/CdSe thin films are prepared by colloidal method and dipping technology using mercaptoethanol (thioglycol) as capping agent. We then investigate the optical characteristics of CdSe QDs and TiO_2/CdSe thin films for application in solar cell devices. Dye-sensitized solar cells based on wide-band gap semiconductors have lower production cost and versatility compared with conventional solid-state cells. We have also prepared CdS/CdSe/ZnS thin films by chemical bath deposition. Results show that TiO_2 mesopores have a wider photoresponse range from the ultraviolet region to the visible light region. To study the effects of co-modification with CdS, CdSe, and ZnS QDs on the photovoltaic response of TiO_2 mesopore-based QD-sensitized solar cell (QDSSC), highly ordered TiO_2 mesopores are fabricated by electrochemical anodization[10]. The TiO_2 mesopores are treated by sequential chemical bath deposition (CBD) of CdS, CdSe, and ZnS QDs and used as photoanodes in QDSSC. We demonstrate that the co-modified TiO_2 mesopores possess superior photovoltaic response compared with single QD-sensitized devices[11]. The TiO_2/CdS/CdSe/ZnS photoanode obtained is a high-efficiency QDSSC.

$Cd(CH_3COO)_2{\cdot}2H_2O$ (99%), dimethyl formamide (C_3H_7NO, 99%), mercaptoethanol (thioglycol, $HOCH_2CH_2SH$, 99%), sodium selenite pentahydrate ($Na_2SeO_3{\cdot}5H_2O$, 98%), acetone, and TiO_2 paste were obtained from Merck. The TiO_2 thin films were fabricated by silk-screen printing with commercial TiO_2 paste. Their sizes ranged from 10 to 20 nm. One layer of film with thickness of 2 μm was printed (measured by Alpha step unit device). Then, the TiO_2 film was heated at 325 °C for 5 min, 375 °C for 5 min, 400 °C for 15 min, and 500 °C for 15 min. Afterward, the film was dipped in 40-mmol $TiCl_4$ solution for 30 min at 70 °C and heated at 500 °C for 30 min.

To prepare TiO_2/CdSe films, the TiO_2 film was dipped in CdSe solution under different time periods to change the thickness of the film. Then, the film was washed three times with acetone. Finally, the film was heated in a vacuum environment at different temperatures to prevent oxidation.

To prepare TiO_2/CdS/CdSe/ZnS films, the highly ordered TiO_2 films were sequentially sensitized with CdS and CdSe QDs by CBD method. First, the TiO_2 film was dipped ino 0.5 mol/L $Cd(CH_3COO)_2$–ethanol solution for 5 min, rinsed with ethanol, dipped for 5 min in 0.5 mol/L Na_2S–methanol solution, and then rinsed with methanol. The two-step dipping procedure corresponded to one CBD cycle, and the incorporated amount of CdS QDs was increased by repeating the assembly cycles for a total of three cycles. For the subsequent CBD process of CdSe QDs, aqueous Se solution was prepared by mixing Se powder and Na_2SO_3 in 50 mL of pure water after adding 1 mol/L NaOH at 70 °C for 7 h. The TiO_2/CdS samples were dipped in 0.5 mol/L $Cd(CH_3COO)_2$–ethanol solution for 5 min at room temperature, rinsed with ethanol, dipped in the Se aqueous solution for 5 min at 50 °C, and rinsed with pure water. The two-step dipping procedure corresponds to one CBD cycle. Repeating the CBD cycle increases the amount of CdSe QDs (a total of four cycles). The CBD method was also used to deposit the ZnS passivation layer. The TiO_2/CdS/CdSe samples were coated with ZnS by alternately dipping the samples in 0.1 mol/L $Zn(NO_3)_2$ and 0.1 mol/L Na_2S solutions twice for 5 min/dip and rinsing with pure water between dips (a total of two cycles). Finally, the samples were heated in a vacuum environment at different temperatures to prevent oxidation (see Fig. 1).

Figure 2 shows the absorption spectra of the CdSe QDs at different M values ($M = Cd^{2+}$/thioglycol). All samples show very strong quantum effects. The peak of the

 © 2013 Chinese Optics Letters

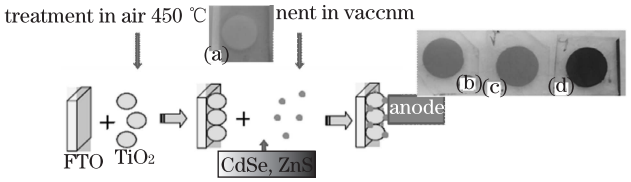

Fig. 1. Preparation of TiO_2/CdS/CdSe/ZnS anode films.

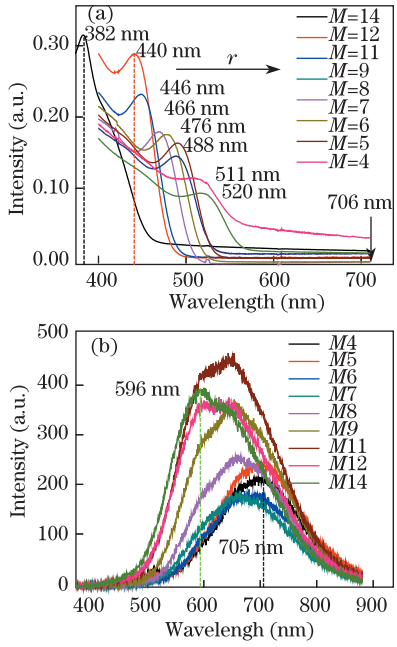

Fig. 2. (Color online) (a) Absorption and (b) photoluminescence spectra of CdSe QDs (M= 4, 5, 6, 7, 8, 9, 11, 12, 14).

Table 1. Describes the Change of the Particle Size on the Concentrate of *M*

Sample	4	5	6	7	8
λ (nm)	520	511	488	488	476
E_g^{eff} (ev)	2.384	2.426	2.540	2.540	2.605
R (nm)	2.471	2.393	2.211	2.211	2.126
Sample		9	11	12	14
λ (nm)		466	446	440	482
E_g^{eff} (ev)		2.660	2.780	2.818	3.246
R (nm)		2.060	1.936	1.901	1.605

absorption spectrum increases from 382 to 520 nm. Thus, the size particle increases from 1.6 to 2.5 nm (Table 1), which is smaller than the radius of Borh (a_B = 5 nm for the CdSe bulk material) as calculated by the approximate equation[12]. This result is related to the shift from light yellow to dark red. Therefore, the CdSe QDs exhibit a strong confinement quantum effect ($R < a_B$)[13]. The -thiol- group, an organic molecule, limits the interaction among CdSe QDs, thereby reducing the link among QDs. The stability of the QDs is due to the movement of the electric charge from the QDs to the ligand field. During this process, thioglycol envelops the newly formed CdSe QDs. When the M value increases, fewer thioglycol groups envelop the QDs. Thus, particle size increases, corresponding to a shift in the peak absorption of light toward the red. The peak of the absorption spectra of the samples is attributed to the shift between two basic excitrons ($1S_{3/2}$–$1S_e$)[12]. The energy shift from 0.6 to 1.2 eV corresponds to the change in the effective radius from 1.6 to 2.5 nm (see Fig. 3), which results from the presence of surface states in the CdSe QDs. The state is the main surface defect inside the QDs, resulting in recombination with electrons. After the electrons are excited from the valence to the conductor band, they immediately return and recombine with the state surface inside the energy gap of the CdSe QDs.

In the Raman spectrum (see Fig. 4), three peaks are observed at 201, 402, and 601 cm^{-1}. These peaks correspond to the phonons of the longitudinal optical vibration in CdSe. The first peak is at 201 cm^{-1} (longitudinal optical, LO). The second peak at 402 cm^{-1} is the second harmonic of the first peak (2LO). The third peak at 601 cm^{-1} is the third harmonic of the first peak. The origin of branch LO and the interactions between the phonons and the surfaces of CdSe QDs depend on the size of the electron-hole pair interaction. Each peak is asymmetrical and tends to stretch toward the low frequency, which is attributed to surface vibration. The LO (201 cm^{-1}) and 2LO (402 cm^{-1}) of the CdSe powder exhibit blueshifting compared with the peaks at 210 and 418 cm^{-1}[1] of the CdSe bulk. Redshifting indicates that CdSe QDs with high area-to-volume ratio are formed in the sample. The Raman spectra of TiO_2/CdSe thin films at different temperatures show the anatase of TiO_2 and the zinc blende of the CdSe structure.

Figure 5(a) is the field emission scanning electron microscopy of the CdSe/TiO_2 anode films that it was conducted at approximately pH 10, and deposition was performed for 24 h at room temperature. With the growth of CdSe, the white TiO_2 film electrode becomes red. After annealing at 300 °C, the film is homogeneous and strongly adherent to the substrate.

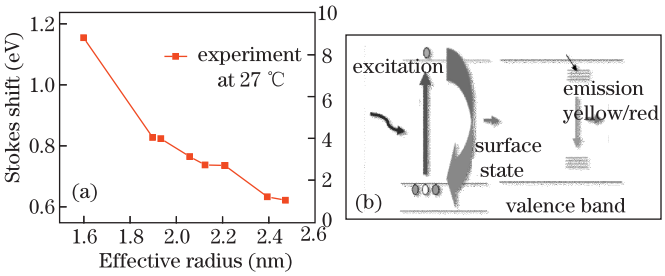

Fig. 3. (a) Energy shift of CdSe at 27 °C depending on the effective radius and (b) surface states in CdSe QDs.

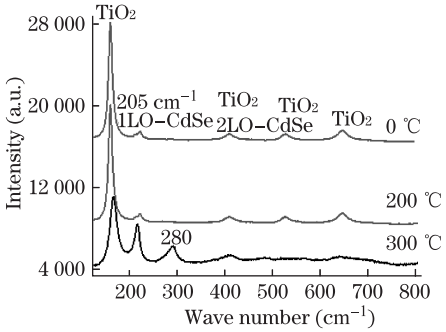

Fig. 4. (Color online) Raman spectra of TiO_2/CdSe thin films at different temperatures.

Table 2 Parameters of Solar Cells with TiO $_2$/CdSe/CdSe (SILAR)/ZnS (SILAR) and TiO $_2$/CdS (SILAR)/CdSe/CdSe (SILAR)/ZnS (SILAR) Anodes

STT	Solar Cell	J_{SC} (mA/cm)^2	V_{OC} (V)	Fill Factor (FF)	Efficiency (η, %)
1	TiO_2/CdSe/CdSe (SILAR)/ZnS (SILAR)	3.688082	0.387615	0.421880	0.603101
2	TiO_2/CdS (SILAR)/CdSe/CdSe (SILAR)/ZnS (SILAR)	7.93295	0.31839	0.419418	1.059354

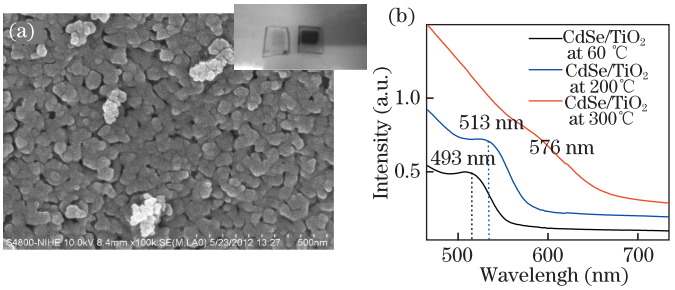

Fig. 5. (Color online) (a) Field emission scanning electron microscopy image and (b) absorption spectrum of the TiO_2/CdSe anode.

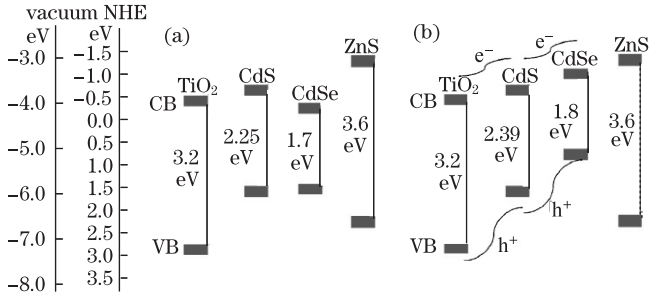

Fig. 6. (a) Relative energy levels of TiO_2, CdS, CdSe, and ZnS in bulk phase; (b) the proposed energy band structure of the TiO_2/CdS/CdSe/ZnS nanostructure interface. All energy levels are based on the normal hydrogen electrode scale. CB and VB are the conduction band and the valence band, respectively[14,15].

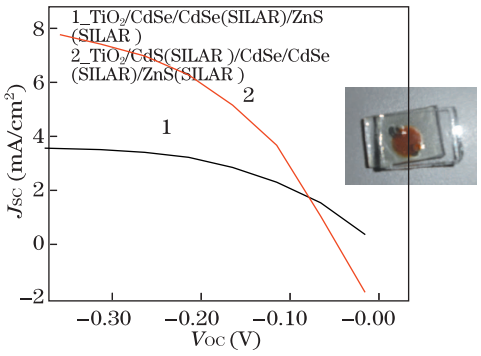

Fig. 7. J-V curves of the solar cell samples with TiO_2/CdSe/CdSe (SILAR)/ZnS (SILAR) and TiO_2/CdS (SILAR)/CdSe/CdSe(SILAR)/ZnS(SILAR) anodes.

Figure 5(a) shows that the surface morphology of the porous TiO_2/CdSe film is smooth and uniform with equally distributed nanometer-sized grains. The absorption spectrum (Fig. 5 (b)) of the self-grown CdSe porous TiO_2 film shows a considerable redshift compared with that of the porous TiO_2, confirming the invasion of CdSe self-grown nanoparticles. As annealing temperature is increased to 300 °C, the CdSe nanocrystals increase in size. The size distribution also increases.

The relative energy level of the different components is shown in Fig. 6(a). According to the data reported in the literature[14,15], the band gap of TiO_2(3.2 eV) limits its absorption range approximately below 400 nm. CdS has a higher conduction band (CB) edge than TiO_2, which is favorable for electron injection. However, with a band gap of 2.25 eV, the absorption of bulk CdS is also limited approximately below 550 nm. Bulk CdSe has a band gap of 1.7 eV, which can extend the absorption to the entire visible region. The CB of CdSe is slightly lower than that of CdS. Lee *et al.* reported that when CdS and CdSe are brought in contact as a cascade structure, the electrons flow from CdS to CdSe[16]. The redistribution of the electrons results in a stepwise band structure. The insertion of a CdS layer between TiO_2 and CdSe elevates the CB of CdSe, generating a higher driving force for electron transportation. In addition, the quantum confinement effect renders the energy level of the CB more negative with decreasing particle size[17]. Thus, a higher efficiency of approximately 0.6031% is obtained with the TiO_2/CdS/CdSe electrode (see Table 2). To improve the photoresponse significantly, two layers of ZnS QDs are coated onto the material. The absorption edge of ZnS is at approximately 345 nm. A higher absorption is thus obtained because the absorption spectrum of ZnS complements those of the CdSe and CdS QDs. Furthermore, ZnS acts as a passivation layer to protect the CdS and CdSe QDs from photocorrosion[18]. The photoexcited electrons efficiently transfer into the CB of TiO_2. The outer ZnS layer is also a potential barrier between the interface of QD materials and electrolyte. ZnS has a very wide band gap of 3.6 eV, which is considerably wider than that of the CdS and CdSe QDs. Therefore, the leakage of electrons from the CdS, CdSe, and ZnS QDs into the electrolyte can be inhibited. The ideal model for the co-sensitized TiO_2 electrode is shown in Fig. 6(b). After the CdS, CdSe, and ZnS QDs are sequentially deposited onto the TiO_2 film, a cascade type of energy band structure is constructed for the co-sensitized photoanode. The best electron transport path is from the CB of ZnS and CdSe to that of CdS, and finally, to TiO_2. This stepwise structure is also favorable for the hole transport, increasing the efficiency of the TiO_2/CdS/CdSe/ZnS electrode. A higher and broader absorption is also obtained, resulting in 1.059354% efficiency (see Fig. 7).

In conclusion, we successfully fabricate a TiO_2 photoanode, which is sequentially modified with CdS, CdSe, and ZnS QDs. The co-sensitized electrode exhibits a significantly improved photoresponse, including wider spectral response range and enhanced efficiency in performance compared with the single-type QD-sensitized electrode. This improvement is mainly attributed to the overlap of the absorption spectra of the different materials and the formation of an ideal stepwise band structure

which promotes the transport of excited electrons and holes across the composite electrode. The synthesized TiO_2/CdS/CdSe/ZnS photoanode exhibits a maximum efficiency value of 1.059354%.

This work was supported by the University of Science of Ho Chi Munh City and Dongthap University.

References

1. L. F. Xi and Y. M. Lam, J. Colloid Interface Sci. **316,** 771 (2007).
2. J. B. Sambur and B. A. Parkinson, J. Am. Chem. Soc. **132,** 2130 (2010).
3. M. H. Chen and L. Gao, J. Am. Ceram, Soc. **88,** 1643 (2005).
4. P.V. Kamat, S. Barazzouk, and S. Hotchandani, Angew. Chem. Int. Ed. **41,** 2764 (2002).
5. M. Zayats, A. B. Kharitonov, S. P. Pogorelova, O. Lioubashevski, E. Katz, and I. J. Willner, Am. Chem. Soc. **125,** 16006 (2003).
6. E. Granot, F. Patolsky, and I. J. Willner, J. Phys. Chem. B **108,** 5875 (2004).
7. R. Baron, C. H. Huang, D. M. Bassani, A. Onopriyenko, M. Zayats, and I. Willner, Angew. Chem. Int. Ed. **44,** 4010 (2005).
8. M. F. Hossain, S. Biswas, Z. H. Zhang, and T. Takahashi, J. Photochem. Photobiol. A **217,** 68 (2011).
9. Z. Li, Y. Xie, H. Xu, T. Wang, Z. Xu, and H. Zhang, J. Photochem. Photobiol. A. **224,** 25 (2011).
10. M. Paulose, K. Shankar, S. oriya, E. Prakasam, O. K. Varghese, G. K. Mor, A. Latempa, A. Fitzgerald, and C. A. Grimes, J. Phys. Chem. B **110,** 16179 (2006).
11. X. F. Gao, W. T. Sun, G. Ai, and L. M. Penga, Appl. Phys. Lett. **96,** 153104 (2010).
12. L. E. Brus. J. Chem. Phys. **80**, 4403 (1984).
13. A. L. Efros, M. Rosen, M. Kuno, M. Nirmal, D. J. Norris. and M. Bawendi, Phys. Rev. B **54,** 4843 (1996).
14. M. Grätzel, Nature **414,** 338 (2001).
15. G. V. Chris and J. Neugebauer, Nature **423**, 626 (2003).
16. Y. L. Lee and Y. S. Lo, Adv. Funct. Mater. **19,** 604 (2009).
17. A. Kongkanand, K. Tvrdy, K. Takechi, M. Kuno, and P. V. Kamat, J. Am. Chem. Soc. **130,** 4007 (2008).
18. Z. Tachan, M. Shalom, I. Hod, S. Ruhle, S. Tirosh, and A. Zaban, J. Phys. Chem. C **115,** 6162 (2011).